THE ASTROPHYSICAL JOURNAL, 510:854–861, 1999 January 10

QUASI-NORMAL MODES OF ROTATING RELATIVISTIC STARS: NEUTRAL MODES FOR REALISTIC EQUATIONS OF STATE

SHARON M. MORSINK
Department of Physics, University of Wisconsin, Milwaukee, P.O. Box 413, Milwaukee, WI 53201; morsink@pauli.phys.uwm.edu
NIKOLAOS STERGIOULAS
Max-Planck-Institute for Gravitational Physics (Albert-Einstein-Institute), D-14473 Potsdam, Germany; niksterg@aei-potsdam.mpg.de
AND
STEVE R. BLATTNIG
Department of Physics, University of Wisconsin, Milwaukee, P.O. Box 413, Milwaukee, WI 53201; srb2@csd.uwm.edu
Received 1998 June 1; accepted 1998 August 18

ABSTRACT

We compute zero-frequency (neutral) quasi-normal f-modes of fully relativistic and rapidly rotating neutron stars using several realistic equations of state (EOSs) for neutron star matter. The zero-frequency modes signal the onset of the gravitational radiation-driven instability. We find that the $l = m = 2$ (bar) f-mode is unstable for stars with gravitational mass as low as 1.0–1.2 $M_\odot$, depending on the EOS. For 1.4 $M_\odot$ neutron stars, the bar mode becomes unstable at 83%–93% of the maximum allowed rotation rate. For a wide range of EOSs, the bar mode becomes unstable at a ratio of rotational to gravitational energies $T/W \sim 0.07$–0.09 for 1.4 $M_\odot$ stars, and $T/W \sim 0.06$ for maximum mass stars. This is to be contrasted with the Newtonian value of $T/W \sim 0.14$. We construct the following empirical formula for the critical value of T/W for the bar mode, $(T/W)_2 = 0.115 - 0.048 M/M_{\rm max}^{\rm sph}$, which is insensitive to the EOS to within 4%–6%. This formula yields an estimate for the neutral mode sequence of the bar mode as a function only of the star's mass M, given the maximum allowed mass $M_{\rm max}^{\rm sph}$, of a nonrotating neutron star. The recent discovery of the fast millisecond pulsar in the supernova remnant N157B supports the suggestion that a fraction of proto–neutron stars are born in a supernova collapse with very large initial angular momentum. If some neutron stars are born in an accretion-induced collapse of a white dwarf, then they will also have very large angular momentum at birth. Thus in a fraction of newly born neutron stars the instability is a promising source of continuous gravitational waves. It could also play a major role in the rotational evolution (through the emission of angular momentum) of merged binary neutron stars if their postmerger angular momentum exceeds the maximum allowed to form a Kerr black hole.

Subject headings: equation of state — instabilities — relativity — stars: neutron — stars: oscillations — stars: rotation

1. INTRODUCTION

A core-collapse supernova or the accretion-induced collapse of a white dwarf can result in the birth of a hot, rapidly rotating neutron star. During the first year of its life (while it cools from $\sim 10^{10}$ to 10^9 K) the neutron star will be unstable to the emission of gravitational radiation due to the Chandrasekhar-Friedman-Schutz (CFS) nonaxisymmetric instability (Chandrasekhar 1970; Friedman & Schutz 1978; Friedman 1978). The instability will only operate while the star is rotating more rapidly than some critical angular velocity. Via the instability, gravitational waves carry away a significant amount of the star's angular momentum. This early spin-down epoch has two important astrophysical implications: first, the gravitational radiation emitted may be detectable by the planned gravitational wave detectors. (Note that this discussion is also relevant to postmerger objects in a neutron star binary coalescence.) Second, it may be possible to indirectly observe the critical angular velocity through the detection of young, rapidly rotating pulsars in supernova remnants such as PSR J0537−6910 (Marshall et al. 1998).

The critical velocity for the onset of the CFS instability in polar perturbations (f-modes) has been computed before in various approximations: in the Newtonian limit (Managan 1985; Imamura, Friedman, & Durisen 1985; Ipser & Lindblom 1990), in the post-Newtonian approximation (Cutler 1991; Cutler & Lindblom 1992; Lindblom 1995), in the relativistic Cowling approximation for polytropes (Yoshida & Eriguchi 1997), and in realistic equations of state (EOSs; Yoshida & Eriguchi 1999).[1] The first fully relativistic computation of the onset of the instability in f-modes is presented in Stergioulas (1996) and Stergioulas & Friedman (1998, hereafter SF98). SF98 find a gauge in which six perturbed field equations can be solved simultaneously on a finite grid with good accuracy. Using polytropic EOSs with index $N = 1.0$, 1.5, and 2.0, SF98 show that general relativity has a significant effect on the onset of the instability, which lowers the rotation rate at which it occurs as the star becomes more relativistic. A surprising result is that the $l = m = 2$, "bar" f-mode instability (which in the Newtonian limit exists only for stiff polytropes of index $N < 0.808$) exists for relativistic polytropes with index as large as $N = 1.3$. SF98 suggested that the $l = m = 2$ instability should also exist for realistic EOSs, which is confirmed in the present paper. In the Newtonian limit the gravitational-wave–driven and viscosity-driven bar mode instabilities occur at the same value of the ratio of rotational energy to

[1] For a detailed review, see N. Stergioulas 1998, Living Reviews in Relativity, 1, available at http://www.livingreviews.org.

the gravitational binding energy, $T/W \sim 0.14$. SF98 conjectured that when effects due to relativity are included, the onset of the two types of instabilities will be split with the CFS instability occurring at lower values of T/W and the viscosity-driven instability at higher values. Calculations of relativistic effects on the viscous instability (Shapiro & Zane 1997; Bonazzola, Frieben, & Gourgoulhon 1998) agree with this conjecture.

For a perturbation with azimuthal angular dependence $e^{im\phi}$, modes with the smallest value of the spherical harmonic multipole index l will have the fastest growth rate and the highest gravitational radiation luminosity. Hence the modes with $l = m$ and, in particular, with $m = 2$ are the most relevant for astrophysics. For a perfect fluid all modes with $m \geq 2$ are of interest; however, when imperfect fluid effects are included (Cutler & Lindblom 1987; Cutler, Lindblom, & Splinter 1990; Ipser & Lindblom 1991; Lindblom 1995; Yoshida & Eriguchi 1995), polar modes with $m > 5$ will always be damped by shear and bulk viscosity.

In the present paper, we use the SF98 scheme to determine the onset of the CFS instability of f-modes with $l = m$, and $2 \leq m \leq 5$ for realistic EOSs. We also improve on the numerical implementation of the method by using a new finite difference scheme in the angular direction and an improved algorithm for locating the exact onset of the instability with higher accuracy. We find that the realistic EOSs show similar behavior as the polytropic EOSs in SF98. The $l = m = 2$ f-mode becomes unstable for all realistic EOSs examined for stars with masses as low as $M = 1.0$–$1.2\ M_\odot$, depending on the EOS. Stars with mass near $1.4\ M_\odot$ are unstable to the bar mode at 83%–93% of the mass-shedding (Kepler) limit.

As was first noticed by Andersson (1998), the critical angular velocity for axial r-modes in a perfect fluid star is exactly zero, so that all stars are generically unstable for all values of m (Friedman & Morsink 1998). Again, the inclusion of viscosity will stabilize all modes except those with the lowest values of m. Two independent computations, including the effects of viscosity in Newtonian stars (Lindblom, Owen, & Morsink 1999; Andersson, Kokkotas, & Schutz 1998), estimate that the lowest angular velocity for which $l = m = 2$ r-mode is unstable is roughly 6%–20% of the Kepler limit for uniformly rotating stars.

The following scenario may describe the early spin evolution of a newly born neutron star if it is born with an angular velocity close to the Kepler limit Ω_K. While the star cools from $\sim 10^{10}$ to 10^9 K, viscous effects will be small enough that the gravitational radiation instability will spin down the star. In this temperature window the spin evolution will go through two phases. In the first phase, the star is rotating fast enough that both f and r-modes will be unstable. During the second phase, only the r-modes are unstable. The determination of which mode will be the dominant mechanism for the shedding of angular momentum during the first phase will depend on the relative growth times for both types of modes. At present, the growth times for either type of mode have not been determined for rapidly rotating relativistic stars.

The plan of this paper is as follows. In § 2 we briefly review the method for computing the onset of the polar mode nonaxisymmetric instability in relativistic stars. In § 3 we present the improvements in the numerical implementation of the scheme. The EOSs selected are discussed in § 4. In § 5 we present the critical angular velocities for f-modes with $2 \leq m \leq 5$ for a variety of EOS. Astrophysical implications will be discussed in the concluding section.

2. NONAXISYMMETRIC PERTURBATIONS

2.1. *Quasi-normal Modes and the Onset of Instability*

Taking advantage of the axisymmetry and stationarity of the equilibrium star, a general linear perturbation can be written as a sum of quasi-normal modes characterized by the spherical harmonic indices (l, m). In this way perturbations of scalars, such as the energy density, can be analyzed as

$$\delta\epsilon = \epsilon_l(r) P_l^m(\cos\theta) e^{i(\omega_i t + m\phi)}\ , \tag{1}$$

where $P_l^m(\cos\theta)$ are the Legendre functions and ω_i is the frequency of the mode in the inertial frame. Perturbations of vector quantities, such as the 4-velocity, can be written in terms of vector harmonics, while the perturbation in the metric can be written in terms of scalar, vector, and tensor harmonics (see Regge & Wheeler 1957). Vector and tensor harmonics are of two types—polar, which transform as $(-1)^l$ under a parity transformation (under the combination of reflection in the equatorial plane and rotation by π), and axial, which transform as $(-1)^{l+1}$ under parity. The angular parts of polar vector harmonics are proportional to gradients of the spherical harmonics, while axial vector harmonics are proportional to the curl of a radial vector and a polar vector harmonic.

In the spherical limit, nonaxisymmetric perturbations decouple into purely polar and purely axial modes with unique values of m and l. In a fluid, polar modes correspond to the f, p, and g-modes in the Newtonian limit, while axial modes correspond to r-modes in a Newtonian star (Papaloizou & Pringle 1978).

In a rotating star, the spherical symmetry is broken. While a mode can still be specified by a single value of m, the mode will no longer consist of a single l harmonic. A polar (l, m) mode acquires higher order in l polar terms owing to the nonsphericity of equipotential surfaces and ($l \pm 1$, m), and higher order in l axial terms owing to the coupling between polar and axial terms:

$$P_l^{\rm rot} \sim \sum_{l'=0}^{\infty} (P_{l+2l'} + A_{l+2l'\pm 1})\ . \tag{2}$$

Similarly, an axial mode in a rotating star is written as a sum of axial and polar terms:

$$A_l^{\rm rot} \sim \sum_{l'=0}^{\infty} (A_{l+2l'} + P_{l+2l'\pm 1})\ . \tag{3}$$

Thus a normal mode of oscillation in a rotating star is defined as polar if it reduces to a purely polar mode in the nonrotating limit and similarly for axial modes.

Gravitational radiation drives a polar or axial mode of oscillation unstable whenever the star rotates fast enough that a perturbation that counterrotates in the star's rest frame appears to corotate with respect to a distant inertial observer. Conservation of angular momentum dictates that the mode's angular momentum must decrease; however, the angular momentum of a counterrotating perturbation (invariantly defined in the rotating frame) is negative so that gravitational radiation causes a negative angular momentum perturbation to become more negative. For a given value of m, the instability first sets in via an $l = m$ mode

when the frequency of the mode vanishes in the inertial frame. Thus the problem of finding the critical angular velocity reduces to finding solutions of the time-independent (zero frequency) perturbation equations.

2.2. *Solving for Time-independent Perturbations*

In this paper we will follow the method of Stergioulas & Friedman (1998), where one can find a detailed presentation. Here we will only briefly sketch the solution method. In § 3 we will summarize improvements in the numerical implementation.

In writing the perturbation equations for an axisymmetric and stationary relativistic star, the Eulerian approach is followed (see Ipser & Lindblom 1992; Friedman & Ipser 1992). The Eulerian perturbations in the metric tensor $\delta g_{ab} \equiv h_{ab}$, energy density $\delta\epsilon$, and 4-velocity δu^a are obtained by solving the system of equations consisting of the perturbed field equations and the perturbed equation of conservation of the stress-energy tensor:

$$\delta R_{ab} = 8\pi(\delta T_{ab} - \tfrac{1}{2} g_{ab}\,\delta T - \tfrac{1}{2} h_{ab}\,T)\,, \tag{4}$$

$$\delta(\nabla_a T^{ab} = 0)\,, \tag{5}$$

where a perfect fluid stress-energy tensor

$$T_{ab} = (\epsilon + P)u^a u^b + P g_{ab} \tag{6}$$

is assumed. In equation (6), ϵ is energy density, P is pressure, and u^a is the 4-velocity of the fluid.

Since linear perturbations are subject to a gauge freedom, only six components of the perturbed field equations need to be solved. The projection of equation (5), normal to the 4-velocity of the fluid (i.e., the perturbed Euler equations), can be solved analytically for δu^a. Next, one defines a function

$$\delta U = u_a\,\delta u^a + \tfrac{1}{2} u^b u^c h_{bc}\,, \tag{7}$$

so that the perturbation in the energy density becomes

$$\delta\epsilon = \frac{(\epsilon + P)^2}{P\Gamma}\left(\delta U + \frac{1}{2}\,u^a u^b h_{ab}\right), \tag{8}$$

where

$$\Gamma = \frac{\epsilon + P}{P}\frac{dP}{d\epsilon} \tag{9}$$

is the adiabatic index of the perturbation (assumed to be equal to the adiabatic index of the equilibrium fluid).

Thus, a zero-frequency mode is obtained by solving six components of the perturbed field (eq. [4]) for h_{ab} and the perturbed energy conservation equation

$$\delta(u_b \nabla_a T^{ab} = 0) \tag{10}$$

for δU. SF98 found that by choosing the gauge as

$$h_{r\theta} = 0\,, \tag{11}$$

$$h_{\theta\phi} = 0\,, \tag{12}$$

$$h_{t\phi} = -\omega h_{\phi\phi}\,, \tag{13}$$

$$h_{\phi\phi} = \frac{h_{\theta\theta}}{r^2}\,e^{2(\psi-\alpha)}\,, \tag{14}$$

six components of the perturbed field equations can be solved simultaneously on a finite grid for the required boundary conditions, given a trial function for δU that is close to its actual solution.

The remaining equation (10) is solved by expanding the function δU in terms of suitably chosen basis functions δU_i,

$$\delta U = \sum_i a_i\,\delta U_i\,. \tag{15}$$

For polar modes, the basis functions are chosen to be

$$\delta U_i = \delta U_i^{(jk)} = r^{l+2(j+k)} Y^m_{l+2k}(\cos\theta)\,, \tag{16}$$

obtained by letting j and k take different values ≥ 0 for each value of i. Equation (10) is an equation linear in δU and can be represented schematically as

$$L(\delta U) = 0\,, \tag{17}$$

where L is the linear operator defined in Appendix C of SF98. Substituting the expansion (eq. [15]) in equation (17), and defining the inner product

$$\langle \delta U_j \,|\, L \,|\, \delta U_i \rangle = \int i\,\frac{\delta U_j}{m\Omega u^t}\,L(\delta U_i)\sqrt{-g}\,d^3x\,, \tag{18}$$

where Ω is the angular velocity of the star, a solution for the homogeneous equation (17) exists only when the determinant of the inner product matrix vanishes,

$$\det\,\langle \delta U_j \,|\, L \,|\, \delta U_i \rangle = 0\,. \tag{19}$$

The solution to the perturbation equations is found by successively solving the perturbed field equations for a trial function of the form given by equation (15), and then evaluating the determinant of equation (18) for a sequence of stars with increasing rotation rate until the determinant's value passes through zero. The star for which the determinant is exactly zero has a zero-frequency (neutral) f-mode, which indicates the onset of the gravitational-radiation–driven instability in this mode.

Stergioulas & Friedman (1998) also found that neutral f-modes can be determined with high accuracy (less than 1% error) in an approximate gauge, in which only two perturbed field equations need to be solved, which allows a larger number of grid points to be used. The approximate gauge is defined by equations (11)–(14), supplemented by the approximations

$$\frac{h_{tt}}{g_{tt} + 2\omega g_{t\phi}} = \frac{h_{rr}}{g_{rr}} = \frac{h_{\theta\theta}}{g_{\theta\theta}} \tag{20}$$

and

$$h_{t\theta} = h_{r\phi} = 0\,. \tag{21}$$

Equation (20) enforces a similar relation between the diagonal components of h_{ab}, as in the Newtonian limit, while equation (21) essentially ignores the axial contribution to the metric perturbation (the axial contribution to the fluid velocity perturbation is retained). All results in the present paper will be obtained using the approximate gauge. Eight basis functions are used in equation (15), which corresponds to $j = 0 \ldots 3$ and $k = 0 \ldots 1$.

3. IMPROVED NUMERICAL IMPLEMENTATION

In SF98, a highly accurate finite-difference scheme was used for the angular variable, which allowed the use of only a few angular spokes. This finite-difference scheme requires the solution to be a very smooth function, and it gave accurate results for relativistic polytropes of index $N \geq 1.0$. Realistic EOSs have, however, a stiff interior and a sudden drop

in density near the surface. Hence the finite difference scheme used in SF98 would suffer from the Gibbs phenomenon at the surface of the star if it were applied to realistic EOSs. This would result in an error of several percent in the determination of neutral modes for these EOSs.

Here we use for the angular variable the same standard 3-point finite difference scheme as is used for the radial variable in SF98. With a fine enough grid, the density distribution near the surface is resolved accurately (see § 4).

Another improvement is the use of Ridder's method (see, e.g., Press et. al. 1992) for locating the exact point along a sequence of rotating stars, where the determinant goes through zero. In SF98, linear interpolation between two nearby stars was used.

4. EQUATIONS OF STATE

The critical neutron star models for a set of EOSs were computed using the method described in the preceding section. Four realistic EOSs, A, C, L, and WFF3, which span a wide range of stiffness, were selected. EOSs A, C, and L are labeled as in Arnett & Bowers (1977). EOS A is one of the softest EOSs that allows a nonrotating 1.4 $M_\odot$ neutron star. EOS C has intermediate stiffness, while EOS L is one of the stiffest realistic EOSs. EOS WFF3 (UV 14 + TNI in Wiringa, Fiks, & Fabrocini 1988) is a modern EOS. At lower densities we match it to an EOS (Lorenz, Ravenhall, & Pethick 1993), which accurately describes the crust of a neutron star (see Nozawa et al. 1998 for more details on the EOSs).

All realistic EOSs examined have an adiabatic index Γ, which is larger than 2.0 at the center and for most of the interior of the star. Thus the equilibrium models are similar to stiff polytropic models with index $N = 1/(\Gamma - 1) < 1.0$. For such polytropic models the Eulerian perturbation in the energy density diverges at the surface. This poses a potential threat to our numerical scheme since the integrand of equation (18) depends on $\delta\epsilon$ (cf., eq. [C24] of SF98). Although the integral (eq. [18]) is formally finite, the divergence of $\delta\epsilon$ at the surface of the star would make it difficult to accurately evaluate the integral. Skinner & Lindblom (1996) avoided this problem by using analytic expressions for the divergence of $\delta\epsilon$ in the case of Newtonian polytropes. In the realistic EOSs that we examined, this problem is not encountered because the EOSs soften near the surface of the star. In Figure 1 we plot the expression $(\epsilon + P)^2/P\Gamma$, which is proportional to $\delta\epsilon$ near the surface, and the adiabatic index Γ as a function of radial coordinate distance (in the equatorial plane) for representative equilibrium models constructed with EOSs C and L. As can be seen, the adiabatic index becomes less than $\Gamma = 2.0$ near the surface, so that $\delta\epsilon$ goes to zero, which occurs in soft polytropes of index $N > 1.0$. With enough grid points in the radial direction, this change in $\delta\epsilon$ can be resolved accurately. Note that $(\epsilon + P)^2/P\Gamma$ has a maximum at *exactly* the points in the interior of the star, where the adiabatic index becomes $\Gamma = 2.0$. The vertical axis in Figure 1 is dimensionless [we set $c = G = 1$ and the length scale equal to $c/(G\epsilon_0)^{1/2}$, where $\epsilon_0 = 10^{15}$ g cm^{-3}].

The critical curves we obtain for the four realistic EOSs are also representative of the critical curves that one would obtain for stiff polytropes if one correctly handled the divergence of $\delta\epsilon$ at the surface or matched a soft polytropic surface to a stiff polytropic interior. For example, models constructed with EOS C are roughly similar to polytropic models of index $N \sim 0.7$, while models constructed with EOS L are roughly similar to polytropic models of index $N \sim 0.5$.

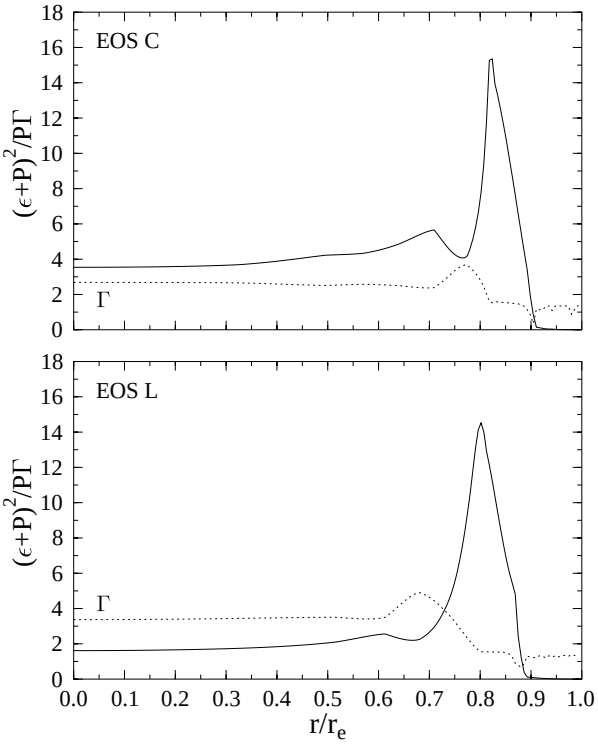

FIG. 1.—Behavior of $(\epsilon + P)^2/P\Gamma$ (*solid line*) and Γ (*dotted line*) in the equatorial plane as a function of coordinate radius (r_e is the coordinate radius at the equator). A 1.44 $M_\odot$ EOS C model (*upper panel*) and a 1.38 $M_\odot$ EOS L model (*lower panel*), which belong to the $l = m = 2$ neutral mode sequence, are shown. The units of the vertical axis are explained in the text. Note that the divergence of $(\epsilon + P)^2/P\Gamma$ at the surface is avoided by a softening of the EOS (Γ becomes less than 2.0).

5. CRITICAL CURVES FOR REALISTIC EQUATIONS OF STATE

Results for each EOS are summarized in Tables 1 and 2 and Figures 2–5. The tables list equilibrium properties of the critical stars for a few selected examples. For each value of m, three stars were selected: a low-mass star, a star with mass close to 1.4 $M_\odot$, and a star close to the maximum mass stable star along each neutral mode sequence. The following quantities are displayed in the tables: central energy density (ϵ_c); ratio of rotational energy to gravitational potential energy (T/W); critical angular velocity (Ω_c); ratio of critical angular velocity Ω_c to the mass-shedding limit Ω_K at same central energy density (Ω_c/Ω_K); gravitational mass (M); rest mass (M_0); and equatorial circumferential radius (R).

The $l = m = 2$ bar mode has the fastest growth time and will be the most efficient mode for the emission of gravitational radiation. For 1.4 $M_\odot$ stars, the bar mode is unstable for $\Omega/\Omega_K > 0.83$ for the softest EOS A, and for $\Omega/\Omega_K > 0.93$ for EOS C. This corresponds to critical spin periods of 0.8 and 1.1 ms for EOSs A and C, respectively. For maximum mass stars the bar mode is unstable for $\Omega/\Omega_K > 0.69$ at $M = 2.9\ M_\odot$ for the stiffest EOS L, and $\Omega/\Omega_K > 0.77$ at $M = 2.0\ M_\odot$ for EOS C.

In terms of T/W, the $l = m = 2$ mode becomes unstable at $T/W \sim 0.071$–0.086 for 1.4 $M_\odot$ stars, and at $T/W \sim 0.06$

TABLE 1

NEUTRAL MODE SEQUENCES FOR EOS A AND EOS L

	ϵ_c ($\times 10^{15}$ g cm^{-3})	T/W	Ω_c ($\times 10^3$ s^{-1})	Ω_c/Ω_K	M ($M_\odot$)	M_0 ($M_\odot$)	R (km)
			EOS A				
$m = 2$.....	1.00	0.082	6.58	0.94	0.97	1.04	12.4
	1.50	0.071	7.46	0.83	1.40	1.55	11.2
	3.20	0.056	9.25	0.72	1.76	2.06	9.4
$m = 3$.....	1.00	0.066	6.02	0.86	0.94	1.00	11.7
	1.60	0.056	6.90	0.74	1.41	1.58	10.7
	3.20	0.044	8.28	0.65	1.73	2.03	9.3
$m = 4$.....	1.00	0.054	5.50	0.79	0.91	0.97	11.3
	1.62	0.045	6.28	0.67	1.40	1.57	10.5
	3.20	0.035	7.42	0.58	1.71	2.00	9.2
$m = 5$.....	1.00	0.044	5.04	0.72	0.89	0.95	11.0
	1.68	0.036	5.80	0.60	1.41	1.58	10.3
	3.20	0.029	6.76	0.53	1.70	1.99	9.1
			EOS L				
$m = 2$.....	0.35	0.089	4.08	0.96	1.20	1.27	18.9
	0.38	0.086	4.20	0.91	1.38	1.48	18.3
	1.20	0.057	5.67	0.69	2.90	3.43	15.1
$m = 3$.....	0.35	0.070	3.70	0.87	1.14	1.21	17.5
	0.40	0.067	3.88	0.81	1.44	1.54	17.2
	1.20	0.045	5.10	0.62	2.85	3.38	14.9
$m = 4$.....	0.35	0.056	3.38	0.79	1.10	1.16	16.8
	0.40	0.054	3.53	0.74	1.39	1.50	16.6
	1.20	0.036	4.58	0.56	2.82	3.34	14.7
$m = 5$.....	0.35	0.046	3.09	0.73	1.08	1.13	16.3
	0.40	0.044	3.23	0.68	1.36	1.46	16.3
	1.20	0.029	4.16	0.51	2.79	3.31	14.6

TABLE 2

NEUTRAL MODE SEQUENCES FOR EOS C AND EOS WFF3

	ϵ_c ($\times 10^{15}$ g cm^{-3})	T/W	Ω_c ($\times 10^3$ s^{-1})	Ω_c/Ω_K	M ($M_\odot$)	M_0 ($M_\odot$)	R (km)
			EOS C				
$m = 2$.....	0.74	0.087	5.48	0.99	1.23	1.32	16.4
	0.90	0.082	5.92	0.93	1.44	1.56	14.9
	2.50	0.059	8.13	0.77	2.00	2.30	11.2
$m = 3$.....	0.70	0.066	4.75	0.89	1.11	1.18	14.9
	0.95	0.061	5.38	0.82	1.43	1.56	13.8
	2.50	0.046	7.30	0.69	1.96	2.26	11.0
$m = 4$.....	0.70	0.052	4.29	0.80	1.07	1.14	14.2
	1.00	0.047	4.94	0.73	1.45	1.58	13.2
	2.50	0.036	6.48	0.62	1.94	2.23	10.8
$m = 5$.....	0.70	0.042	3.91	0.73	1.05	1.11	13.8
	1.00	0.038	4.46	0.65	1.42	1.55	12.9
	2.50	0.028	5.79	0.55	1.92	2.20	10.7
			EOS WFF3				
$m = 2$.....	0.80	0.091	6.09	0.98	1.10	1.17	14.6
	1.00	0.083	6.56	0.89	1.40	1.53	13.2
	2.50	0.059	8.33	0.74	1.98	2.31	10.7
$m = 3$.....	0.70	0.072	5.17	0.94	0.86	0.90	13.9
	1.05	0.063	5.99	0.79	1.40	1.55	12.5
	2.50	0.046	7.44	0.66	1.95	2.27	10.5
$m = 4$.....	0.70	0.057	4.68	0.85	0.82	0.87	13.0
	1.10	0.051	5.55	0.71	1.43	1.58	12.1
	2.50	0.037	6.73	0.60	1.92	2.24	10.4
$m = 5$.....	0.70	0.047	4.31	0.79	0.80	0.85	12.6
	1.10	0.042	5.09	0.65	1.40	1.55	11.8
	2.50	0.031	6.18	0.55	1.91	2.23	10.3

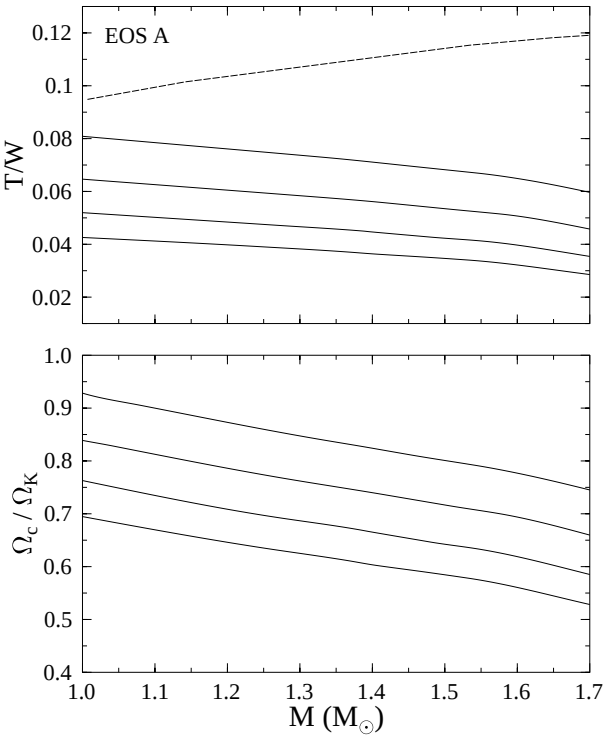

FIG. 2.—Neutral mode sequences for EOS A. Shown are the ratio of rotational to gravitational energy T/W (*upper panel*) and the ratio of the critical angular velocity Ω_c to the angular velocity at the mass-shedding limit for uniform rotation (*lower panel*) as a function of gravitational mass. The solid lines are the neutral mode sequences for $l = m = 2$, 3, 4, and 5 (*from top to bottom*), while the dashed line in the upper panel corresponds to the mass-shedding limit for uniform rotation.

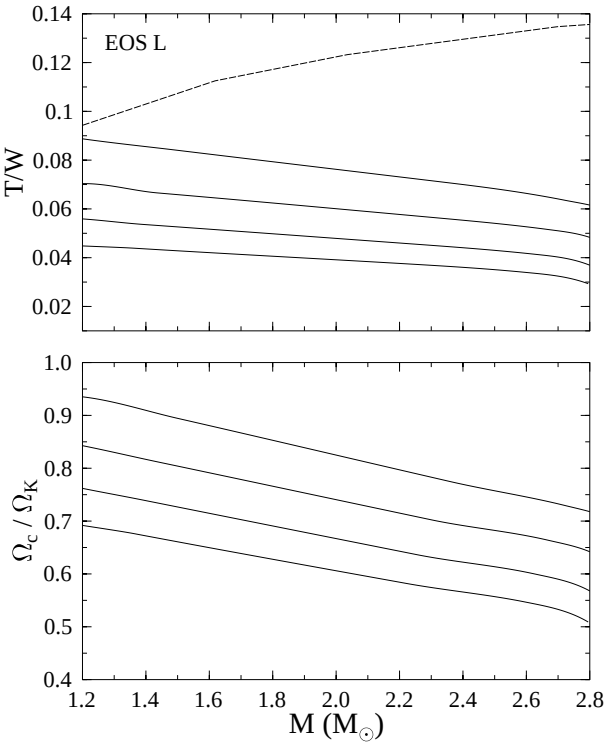

FIG. 3.—Same as Fig. 2, but for EOS L

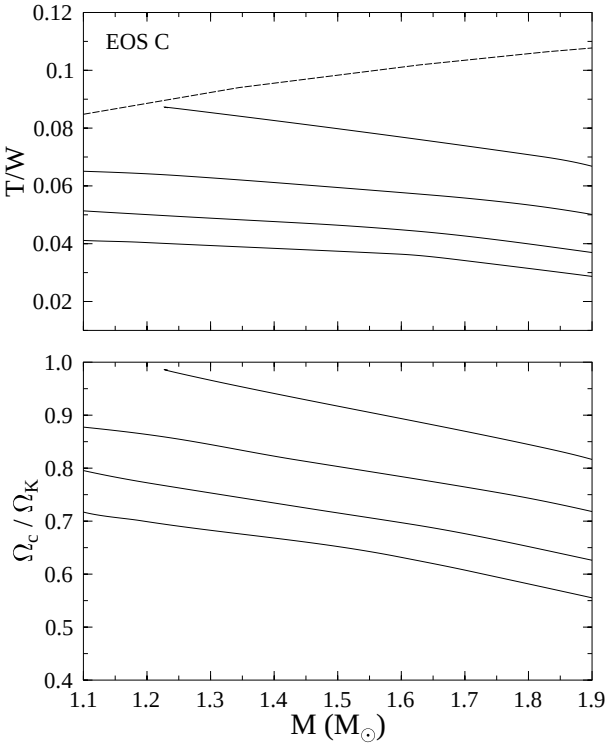

FIG. 4.—Same as Fig. 2, but for EOS C

for the maximum mass along the neutral mode sequence. The latter value is surprisingly insensitive to the EOS. In fact, the $l = m = 2$ neutral mode sequence can be approximated by the following linear empirical formula:

$$\left(\frac{T}{W}\right)_2 = 0.115 - 0.048\,\frac{M}{M_{\rm max}^{\rm sph}}\,, \tag{22}$$

where $M_{\rm max}^{\rm sph}$ is the maximum mass for a spherical star allowed by a given EOS. The empirical formula has an accuracy of roughly 4%–6% for all values of M except for stars near the axisymmetric stability limit; that is, near the maximum mass along the neutral mode sequence where it is somewhat larger (the T/W vs. M curves deviate somewhat from linearity, as can be seen in Figs. 2–5). While in the Newtonian limit the bar mode becomes unstable at $T/W \sim 0.14$, in realistic 1.4 $M_\odot$ neutron stars the onset of the bar mode instability is at roughly one-half to two-thirds the Newtonian estimate of T/W.

The critical curves for the $l = m = 3$, 4, and 5 modes appear at successively lower rotation rates. All critical curves for all EOSs are nearly linear in gravitational mass, and similar empirical formulae for these modes can also be written as in equation (22).

The obtained critical curves assume a perfect fluid. We expect that including the effects of viscosity will raise the critical angular velocities by a few percent in the 10^9–10^{10} K temperature window. The strengthening of the instability by relativistic effects will also widen the temperature window in which the instability will be active, as was already shown by post-Newtonian computations (Cutler & Lindblom 1992; Lindblom 1995).

By doubling the number of grid points in both directions, and from comparisons with the Newtonian limit and with the results in SF98, we estimate the accuracy of our present

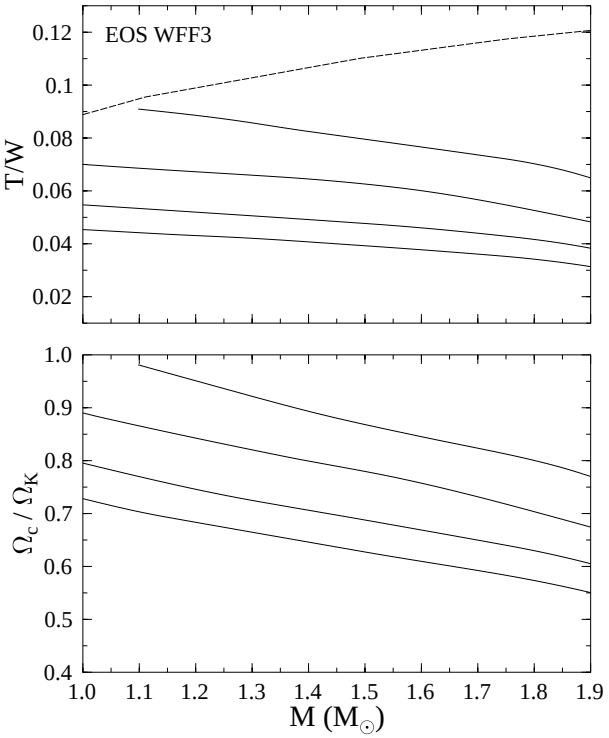

FIG. 5.—Same as Fig. 2, but for EOS WFF3

results to be at the 1% level. Increasing the number of basis functions in equation (15) to more than eight did not affect the critical curves by more than 1%.

6. DISCUSSION

We find that for a wide range of realistic EOSs the polar $l = m = 2$ bar mode is unstable to the emission of gravitational waves in newly born 1.4 $M_\odot$ neutron stars, rotating close to the Kepler limit until their angular velocity falls below 83%–93% of the Keplerian value. The recent observation of the fastest rotating young pulsar in the supernova remnant N157B (Marshall et al. 1998) suggests that a fraction of neutron stars born in supernovae are born with very large initial rotational energy. If some neutron stars are born in accretion-induced collapse of white dwarfs (Friedman 1983), they are also expected to have a large initial spin. Since it is initially very hot and differentially rotating, a proto–neutron star can even be born with an angular velocity exceeding the mass-shedding limit for uniformly rotating stars. As the star cools and passes through the temperature window of 10^9–10^{10} K, the nonaxisymmetric bar mode, driven by gravitational radiation, will grow and the star will lose angular momentum by the emission of gravitational waves. Within a short time the star will have slowed down enough that the bar mode will become stable again. At this point, viscosity changes the density profile of the star to a nearly axisymmetric configuration (see Lai & Shapiro 1995 for a recent discussion), but higher order mass and equal or higher order current multipoles may still be present. During this first phase the *r*-mode instability will also be operating. The *r*-mode instability will then continue to slow down the star until the star reaches a period of roughly 6–9 ms, when the instability will be damped by viscosity.

The above picture assumes that the star cools through the standard modified URCA cooling scenario. If instead neutron stars cool very rapidly through, e.g., the direct Urca process, then the instability in *f*-modes may not have enough time to grow significantly, and the rotational evolution of the star will only be affected by the *r*-mode instability.

The results presented in this paper confirm that general relativity decreases the critical value of T/W for the gravitational-wave–driven instability, as suggested by SF98. Combined with the observation (Shapiro & Zane 1997; Bonazzola et. al. 1998) that the effect of general relativity on the onset of the viscous instability is to make it occur at higher values of T/W, it is clear that the CFS instability is more likely to occur than the viscous instability. The increase in the critical value of T/W for the onset of viscous instability can be understood on intuitive grounds. The viscous instability is essentially a battle between gravity, which acts to keep the fluid centrally condensed and a centrifugal "force" that acts to drive the fluid away from the center of the star. The role of viscosity is to act as a vehicle for the centrifugal force to overcome gravity's attraction. (This is similar to the mechanical example of a bead on a vertical U-shaped wire. When the wire is static, the bead sits at the bottom of the U. When the wire rotates about a vertical axis, the bead will move up to a higher equilibrium position on the wire if there is friction between the bead and the wire.) As a sequence of stars becomes more relativistic, the gravitational field is stronger and the viscous instability can only set in when the centrifugal force is larger; i.e., for larger values of T/W. It is more difficult to explain why the CFS instability sets in at lower values of T/W for general relativity than for Newtonian gravity. We note that in the Cowling approximation (S. Yoshida & Y. Eriguchi 1998, private communication) the frequencies of the *f*-modes decrease as the compactness of the stars increase. Similarly, our figures show that T/W for the onset of the instability decreases as the compactness increases. Since Newtonian gravity underestimates the compactness of a neutron star, it seems likely that it also overestimates the value of T/W for the neutral mode.

The CFS-instability in the bar *f*-mode appears to be a good source of detectable continuous gravitational waves. Lai & Shapiro (1995) have studied the development of the *f*-mode instability using Newtonian ellipsoidal models of rotating stars (Lai, Rasio, & Shapiro 1993, 1994). They consider the case where a neutron star is created in a core collapse with large initial angular momentum. After a brief dynamical phase, the proto–neutron star becomes axisymmetric but secularly unstable. The instability deforms the star into a nonaxisymmetric configuration via the $l = m = 2$ bar mode. As the star slows down, the frequency of the gravitational waves sweeps downward from a few hundred to 0 Hz, passing through the ideal sensitivity band of LIGO. A rough estimate of the wave amplitude shows that at $\sim$100 Hz the gravitational waves from the CFS instability could be detected out to the distance of 30 Mpc by LIGO or VIRGO, and to 140 Mpc by the advanced LIGO detector. This result is very promising, especially since for relativistic stars the instability will be stronger than in the Newtonian computations.

Another astrophysical situation in which the instability may have the opportunity to grow is after the merger of two neutron stars in a binary coalescence. Recently, Baumgarte

& Shapiro (1998) studied the case in which the merged neutron star is unstable to collapse but has more angular momentum than required to collapse to a Kerr black hole. They find that neutrino emission is inefficient for shedding the excess angular momentum of the neutron star, and they suggest that this can happen through the growth of the gravitational-radiation–driven bar f-mode. We expect the gravitational waves from the instability in these high-mass ($M > 2.8\ M_{\odot}$) merged neutron stars to be especially strong and a detailed, full, relativistic study is needed.

The computation of quasi-normal finite-frequency modes of rapidly rotating relativistic stars is a more difficult problem than the neutral-mode calculation presented in this paper. The main difficulty is in applying the boundary conditions at infinity. Lindblom, Mendell, & Ipser (1997) have recently proposed an approximate near-zone boundary condition that appears to be a promising approach for solving for the complex eigenfrequencies. We plan to incorporate the near-zone boundary conditions into the SF98 method to allow the approximate computation of frequencies and growth times of the quasi-normal modes with reasonable accuracy.

It is a pleasure to thank John Friedman for helpful discussions, and Nils Andersson for a critical reading of the manuscript. We also thank S. Yoshida and Y. Eriguchi for providing us with graphs of critical curves for two realistic EOSs obtained in the Cowling approximation before their publication. N. S. and S. M. M. acknowledge the generous hospitality of the Max-Planck-Institute for Gravitational Physics (Albert-Einstein-Institute) in Potsdam, Germany. This work was supported in part by NSF grant PHY 95-07740 and by NSERC of Canada.

REFERENCES

Andersson, N. 1998, ApJ, 502, 708
Andersson, N., Kokkotas, K., & Schutz, B. F. 1998, preprint (gr-qc/9805225)
Arnett, W. D., & Bowers, R. L. 1977, ApJS, 33, 415
Baumgarte, T. W., & Shapiro, S. L. 1998, ApJ, 504, 431
Bonazzola, S., Frieben, J., & Gourgoulhon, E. 1998, A&A, 331, 280
Chandrasekhar, S. 1970, Phys. Rev. Lett., 24, 611
Cutler, C. 1991, ApJ, 374, 248
Cutler, C., & Lindblom, L. 1987, ApJ, 314, 234
———. 1992, ApJ, 385, 630
Cutler, C., Lindblom, L., & Splinter, R. J. 1990, ApJ, 363, 603
Friedman, J. L. 1978, Commun. Math. Phys., 62, 247
———. 1983, Phys. Rev. Lett., 51, 11
Friedman, J. L., & Ipser, J. 1992, Philos. Trans. R. Soc. London, A, 340, 391
Friedman, J. L., & Morsink, S. M. 1998, ApJ, 502, 714
Friedman, J. L., & Schutz, B. F. 1978, ApJ, 222, 281
Imamura, J. N., Friedman, J. L., & Durisen, R. H. 1985, ApJ, 294, 474
Ipser, J. R., & Lindblom, L. 1990, ApJ, 355, 226
———. 1991, ApJ, 373, 213
———. 1992, ApJ, 389, 392
Lai, D., Rasio, F. A., & Shapiro, S. L. 1993, ApJS, 88, 205
———. 1994, ApJ, 373, 213
Lai, D., & Shapiro, S. L. 1995, ApJ, 442, 259
Lindblom, L. 1995, ApJ, 438, 265
Lindblom, L., Mendell, G., & Ipser, J. R. 1997, Phys. Rev. D, 56, 2118
Lindblom, L., Owen, B. J., & Morsink, S. M. 1998, Phys. Rev. Lett., 80, 4843
Lorenz, C. P., Ravenhall, D. G., & Pethick, C. J. 1993, Phys. Rev. Lett., 70, 379
Managan, R. A. 1985, ApJ, 294, 463
Marshall, F. E., Gotthelf, E. V., Zhang, W., Middleditch, J., & Wang, Q. D. 1998, ApJ, 499, L179
Nozawa, T., Stergioulas, N., Gourgoulhon, E., & Eriguchi, Y. 1998, A&A, 132, 431
Papaloizou, J., & Pringle, J. E. 1978, MNRAS, 182, 423
Press, W. H., Teukolsky, S., Vetterling, W. T., & Flannery, B. P. 1992, Numerical Recipes in C (2d ed.; Cambridge: Cambridge Univ. Press)
Regge, T., & Wheeler, J. A. 1957, Phys. Rev., 108, 1063
Shapiro, S. L., & Zane, S. 1997, preprint (gr-qc/9711050)
Skinner, D., & Lindblom, L. 1996, ApJ, 461, 920
Stergioulas, N. 1996, Ph.D. thesis, Univ. of Wisconsin, Milwaukee
Stergioulas, N., & Friedman, J. L. 1998, ApJ, 492, 301
Wiringa, R. B., Fiks, V., & Fabrocini, A. 1988, Phys. Rev., 38, 1010
Yoshida, S., & Eriguchi, Y. 1995, ApJ, 438, 830
———. 1997, ApJ, 490, 779
———. 1999, ApJ, submitted